AD-A072 509   NAVAL OCEAN SYSTEMS CENTER SAN DIEGO CA   F/G 9/2

PROCESSING AND DISPLAY TECHNIQUES FOR MULTISPECTRAL SATELLITE I--ETC(U)

APR 79   J A ROESE

UNCLASSIFIED   NOSC/TR-439   NL

1 OF 1

AD

A072509

END

DATE

FILMED

9 - 79

DDC

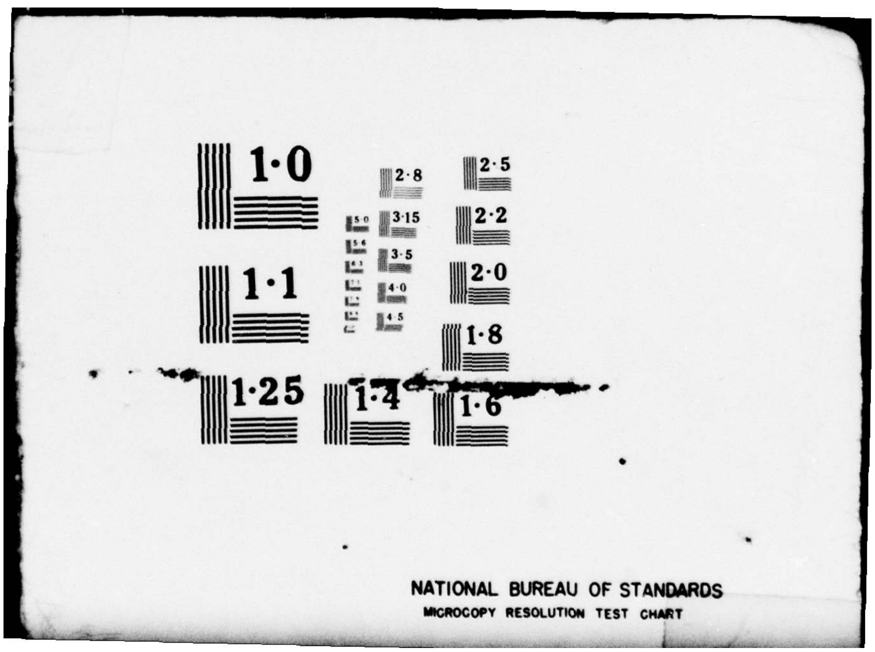
1·0
1·1
1·25
1·4
1·6
1·8
2·0
2·2
2·5
2·8
3·15
3·5
4·0
4·5
NATIONAL BUREAU OF STANDARDS
MICROCOPY RESOLUTION TEST CHART

LEVEL II

(12)

NOSC

NOSC TR 439

NOSC TR 439

Technical Report 439

PROCESSING AND DISPLAY TECHNIQUES FOR MULTISPECTRAL SATELLITE IMAGERY

JA Roese

April 1979

Final Report: 1 February — 30 September 1978

NAVAL OCEAN SYSTEMS CENTER
SAN DIEGO, CALIFORNIA 92152

NAVAL OCEAN SYSTEMS CENTER, SAN DIEGO, CA 92152

AN ACTIVITY OF THE NAVAL MATERIAL COMMAND

RR GAVAZZI, CAPT, USN
Commander

HL BLOOD
Technical Director

ADMINISTRATIVE INFORMATION

This report summarizes work performed for the FY78 IR/IED Satellite Image Processing Program, Program Element 61152N, Task ZR014-08. This work was performed during the period February through September, 1978.

Released by
DA Hanna, Head
Signal Processing and
Display Division

Under authority of
HA Schenk, Head
Undersea Surveillance Department

UNCLASSIFIED

SECURITY CLASSIFICATION OF THIS PAGE (When Data Entered)

REPORT DOCUMENTATION PAGE

READ INSTRUCTIONS BEFORE COMPLETING FORM

1. REPORT NUMBER Technical Report 439 (TR 439)	2. GOVT ACCESSION NO.	3. RECIPIENT'S CATALOG NUMBER
4. TITLE (and Subtitle) 6 Processing and Display Techniques for Multispectral Satellite Imagery,		5. TYPE OF REPORT & PERIOD COVERED Final: 1 February - 30 September 1978 6. PERFORMING ORG. REPORT NUMBER
7. AUTHOR(s) 10 J.A. Roese		8. CONTRACT OR GRANT NUMBER(s)
9. PERFORMING ORGANIZATION NAME AND ADDRESS Naval Ocean Systems Center San Diego, CA 92152	393 159	10. PROGRAM ELEMENT, PROJECT, TASK AREA & WORK UNIT NUMBERS 61152N, ZR014-08
11. CONTROLLING OFFICE NAME AND ADDRESS Naval Ocean Systems Center San Diego, CA 92152	11	12. REPORT DATE April 1979 13. NUMBER OF PAGES 37
14. MONITORING AGENCY NAME & ADDRESS(if different from Controlling Office) 12 40p.		15. SECURITY CLASS. (of this report) Unclassified 15a. DECLASSIFICATION/DOWNGRADING SCHEDULE

16. DISTRIBUTION STATEMENT (of this Report)

Approved for public release; distribution unlimited

9 Final rept. 1 Feb-30 Sep 78,

17. DISTRIBUTION STATEMENT (of the abstract entered in Block 20, if different from Report)

14 NOSC/TR-439 16 ZR01408

18. SUPPLEMENTARY NOTES

ORIGINAL CONTAINS COLOR PLATES: ALL DDC REPRODUCTIONS WILL BE IN BLACK AND WHITE

19. KEY WORDS (Continue on reverse side if necessary and identify by block number)

Digital image processing
Display systems
Multispectral imagery
Remote sensors
Satellite imagery
Stereoscopic displays

20. ABSTRACT (Continue on reverse side if necessary and identify by block number)

In recent years, the technology area of remote sensing by multispectral satellite sensors has evolved greatly. Imagery obtained by satellite means has been the basis for much work in the areas of environmental studies, resource planning, terrain mapping, weather prediction and military reconnaissance. This program effort has investigated the application of various image processing and display techniques for use with multispectral satellite imagery. Emphasis has been placed on the development and implementation of two-dimensional processing techniques applied in the domain of the original image. Two-dimensional transform domain image processing and display techniques were also adapted for use with satellite imagery.

DD FORM 1 JAN 73 1473 EDITION OF 1 NOV 65 IS OBSOLETE
S/N 0102-LF-014-6601

UNCLASSIFIED 393 159

SECURITY CLASSIFICATION OF THIS PAGE (When Data Entered)

OBJECTIVES

1. Investigate utility of two-dimensional image processing and display techniques for use with multispectral satellite imagery.

2. Where appropriate, incorporate for application to satellite imagery the two-dimensional transform and linear/nonlinear image domain processing and display concepts previously developed for acoustic signal space displays.

RESULTS

1. Linear and nonlinear image domain processing techniques have been shown to produce enhanced representations of multispectral satellite imagery.

2. Two-dimensional Fourier transform processing has been successfully applied to cloud structure analysis of satellite imagery.

3. The adaptation of field-sequential stereoscopic techniques for displaying composite visible/infrared spectrum satellite images has been successfully demonstrated.

4. The use of a three-coordinate cursor as an interactive aid for determining cloud height and temperature information has been shown to have potential for meteorological image analysis applications.

RECOMMENDATIONS

1. Continue to develop and refine two-dimensional image processing algorithms for the enhancement and display of multispectral satellite imagery.

2. Investigate alternative display techniques for the simultaneous presentation of visible and infrared as well as other combinations of remotely sensed spectral imagery.

CONTENTS

SECTION 1. INTRODUCTION

In recent years, the technology area of remote sensing by satellite-borne sensors has evolved greatly. Imagery obtained by satellite has been the basis for much work in the areas of environmental studies, resource planning, terrain mapping, weather analysis and military reconnaissance. These activities have been aided by the fact that many satellite sensors provide geographically coincident scans in multiple spectral bands including visible for sensing reflectivity and infrared (IR) for recording thermal information.

The manner in which multispectral imagery is processed and displayed to the user is important to the ultimate analysis and interpretation of satellite imagery. The purpose of this program effort has been to investigate the utility of various image processing and display techniques for use with multispectral satellite imagery. The program emphasis has been on the development and implementation of two-dimensional techniques applied in the domain of the original image. Where appropriate, transform domain image processing and display concepts previously developed for acoustic signal space displays were also adapted for application to satellite imagery.

A major program objective was the establishment of a data set of representative multispectral satellite imagery. Satellite images obtained during the course of this effort were taken from the following satellite platforms: Defense Meteorological Satellite Program (DMSP); Nimbus 6; National Oceanographic and Atmospheric Administration (NOAA) 5 weather satellite; Synchronous Meteorological Satellites (SMS) 1 and 2; and from a Pioneer deep space probe flyby of Venus. Images from this data set are used in the body of this report as examples illustrating the operations of the image processing and display techniques investigated.

The display and processing resources of the NOSC Display and Image Processing Laboratory were used in obtaining the results presented in this report. A description of this laboratory is given in appendix A.

SECTION 2. SATELLITE IMAGE PROCESSING TECHNIQUES

An extensive set of processing techniques exists for the enhancement of two-dimensional digital imagery. These techniques include operations performed in the spatial domain of the original image as well as operations which require transform domain representations in terms of the spatial frequency content of the image.

The techniques discussed in this section include both linear and nonlinear spatial domain processing methods and two-dimensional Fourier transforms for spatial frequency domain image representations. The techniques investigated were selected on the basis of the effectiveness for image enhancement and analysis operations and on their computational requirements.

INTENSITY SCALING

A common source of low image quality is poor contrast resulting from a limited dynamic range of recorded sensor data values. A powerful technique for improving or enhancing contrast within an image is to rescale the sensor data values for each discrete picture element (pixel) of the displayed image.

Linear, piecewise linear, and nonlinear mappings can be used to perform intensity rescaling. Piecewise linear and nonlinear mappings are of particular interest because relatively large portions of the pixel intensity dynamic range can, for example, be allocated to the display of a small range of high interest data values in the original image. In addition, on-line assignments of these mappings can be made for operations involving imagery analysis performed in an interactive mode.

An original NOAA visible spectrum satellite image is shown in figure 2-1 (a). For comparison purposes linear, piecewise linear, and nonlinear rescaling mapping of the NOAA image are also illustrated as figures 2-1 (b) through 2-1 (d). The rescaled images demonstrate that improvements in perceived image detail can be achieved as a result of intensity rescaling. Frequency histograms for the images in figure 2-1 are given in figures 2-2 (a) through 2-2 (d). In the frequency histograms, the range of sensor data values for the original image is shown along the X axis. These data values are typically biased above zero with a dynamic range which is generally not well matched to the 64-level dynamic range of the CRT display device shown on the Y axis. In these examples, the distribution of data values for the original image is determined by computing the image frequency histogram which is a measure of the number of occurrences of each data value within an image and provides a probability distribution of the image data values. The limits of the nonzero entries in the frequency histogram give the dynamic range of the image data values.

Figure 2-1 (a) shows the original NOAA visible spectrum image, while figure 2-2 (a) illustrates the corresponding frequency histogram with a standard linear intensity mapping. From these figures, it can be seen that the original image data values are mapped into only a subset of the available pixel display intensities. Thus the dynamic range of the CRT display device is not fully utilized for displaying the original image data.

An improvement in the contrast of the NOAA image is achieved by the use of a linear mapping which is matched to the range of the original image data values. This situation is illustrated in figures 2-1 (b) and 2-2 (b) where a linear mapping extending from the minimum to the maximum data values in the original image is used. The effect of this type of simple linear intensity rescaling for contrast enhancement can be seen by noting the presence of background land masses in figure 2-1 (b) which were not observed in the original image of figure 2-1 (a).

Further enhancements in selected segments of the original NOAA image can be achieved with piecewise linear mappings. For example, the multiple mode nature of the image frequency histogram can be directly attributed to data values generated by the large water, land, and cloud masses in the original data image. A piecewise linear mapping was selected to increase the portion of the display device dynamic range assigned to the lower intensity water and land regions of the image at the expense of the remaining cloud areas. The result of this piecewise linear mapping is shown in figure 2-1 (c).

A powerful nonlinear rescaling technique is histogram equalization. The histogram equalization procedure rescales image data values such that the frequency histogram of the adjusted image is approximately uniform. In an image with a uniform histogram, the fraction of the total number of pixels at each data value is nearly equal. The algorithm for rescaling the data values of the original image for histogram equalization is

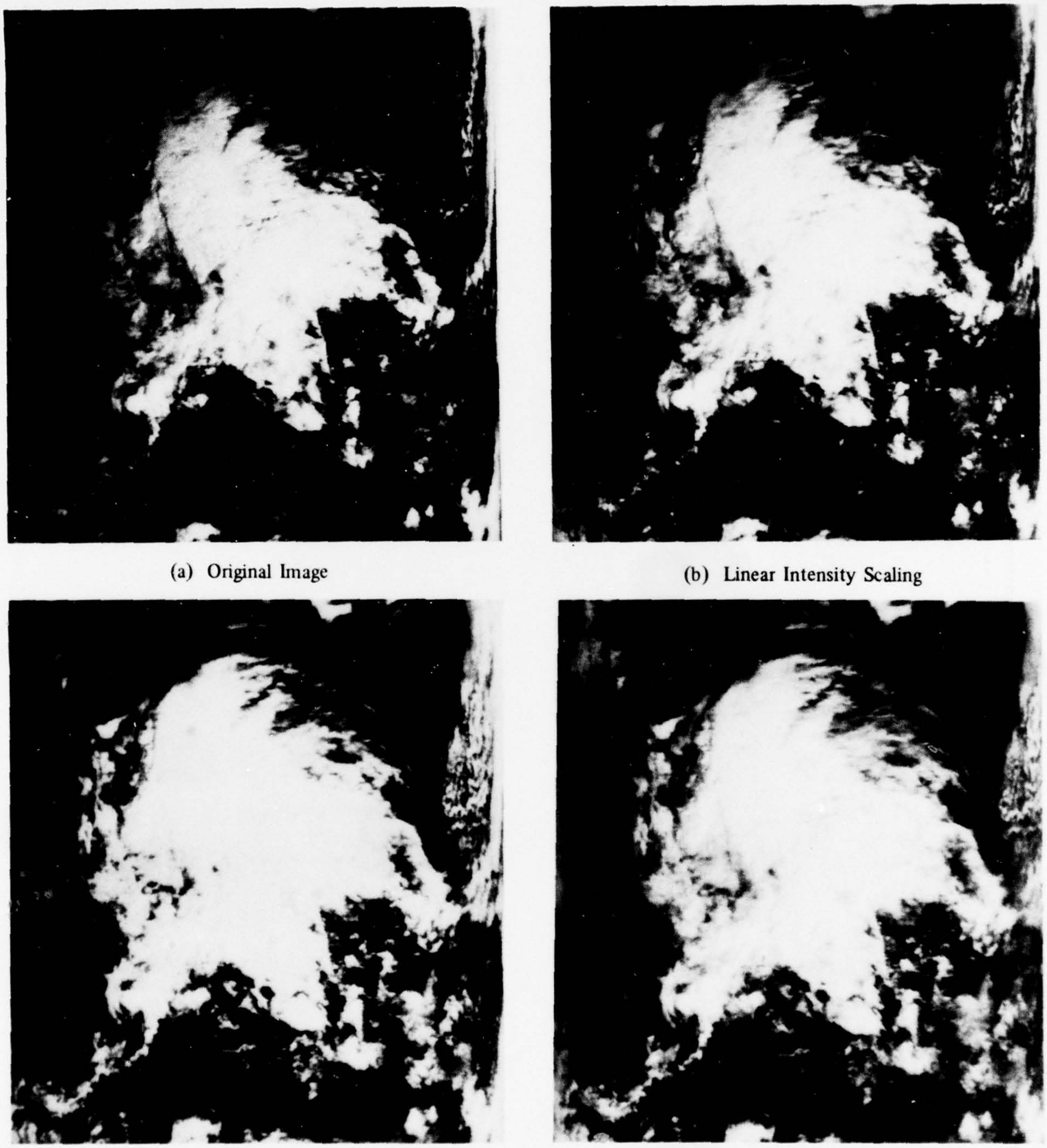

(a) Original Image

(b) Linear Intensity Scaling

(c) Piecewise Linear Intensity Scaling

(d) Histogram Equalization

Figure 2-1. Comparison of original NOAA visible spectrum image with linear, piecewise linear, and nonlinear (histogram equalized) intensity scaled images.

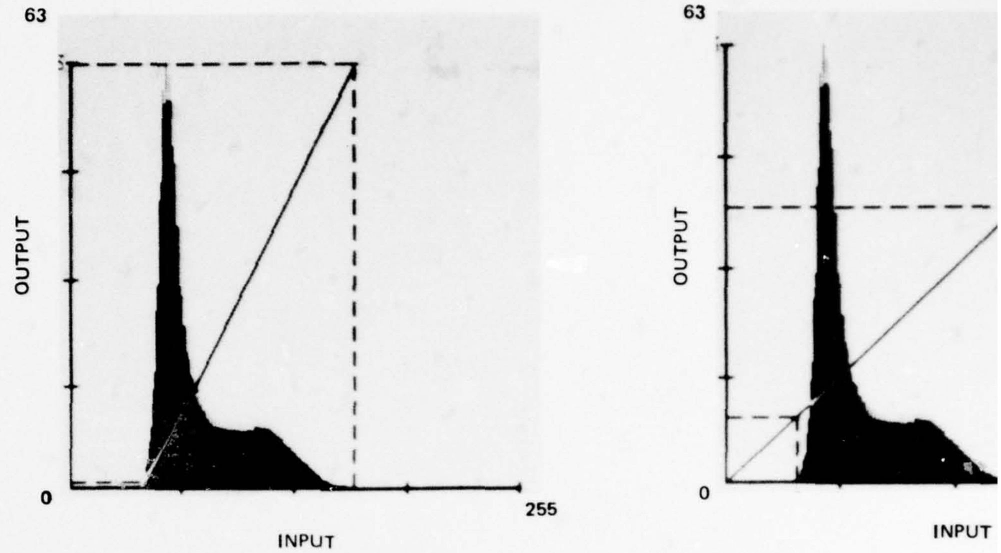

(a) Standard Linear Intensity Mapping

(b) Modified Linear Int

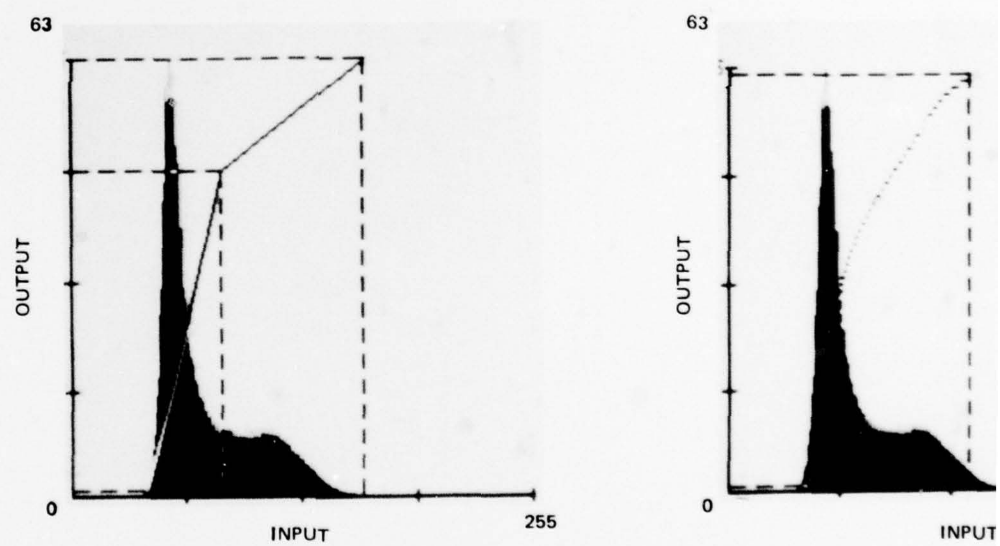

(c) Piecewise Linear Intensity Mapping

(d) Nonlinear Inte

Figure 2-2. Comparison of frequency histograms for NOAA visible spectrum satellite image for st linear, piecewise linear, and nonlinear (histogram equalized) intensity mappings.

computationally simple. The pixels with the lowest data values are grouped together until their population approximately equals the desired fraction of pixels assigned to the first intensity level of the scaled image. These pixels are then assigned this intensity value. The process is then repeated for the remaining pixels of the original image. In order for the histogram equalization process to properly assign all pixels with the same data values to the same intensity level, the number of intensity levels in the rescaled image must be less than the number of data values in the original image. In situations where the number of levels in the original and rescaled images is the same, random redistribution procedures must be employed to resolve intensity rescaling ambiguities.

Figure 2-1 (d) illustrates the NOAA satellite visible spectrum image with rescaling to achieve an approximately uniform histogram. The mapping from the data values in the original image to the 64 intensity levels for the CRT display device is illustrated in figure 2-2 (d). Histogram equalization for this image results in an effective utilization of the CRT display dynamic range that permits the observer to simultaneously view all data values within the original image.

Histogram equalization is a useful tool in the analysis of natural images, since the distribution of pixel data values is often skewed toward the lower levels. Images with skewed distributions can obscure detail within the lower data value regions. Rescaling using histogram equalization techniques will often improve the visual perception of detail within an image.

NONLINEAR EDGE DETECTION

A common requirement in the analysis of remotely sensed imagery is the detection of edges or boundaries of intensity transitions. A frequently used class of image edge detectors is based on nonlinear combinations of intensity values using adjacent sets of four or nine pixels.

A simple square root edge detection technique is the Roberts[1] cross operator for 2 X 2 regions of an image. The Roberts cross operator is basically a two-dimensional differencing technique and is defined as

$$R_{SR}(x,y) = \left([I(x,y) - I(x+1, y+1)]^2 + [I(x, y+1) - I(x+1, y)]^2 \right)^{1/2} \quad (2\text{-}1)$$

where $I(x,y)$ is the pixel intensity value at location x,y and $R_{SR}(x,y)$ is the edge detection measure. A simplified form of the Roberts cross operator requiring only the computation of magnitudes of differences between adjacent pixel intensities is given by

$$R_M(x,y) = \left| I(x,y) - I(x+1, y+1) \right| + \left| I(x, y+1) - I(x+1, y) \right| \quad (2\text{-}2)$$

An extension of the four-element differencing techniques used in the Roberts cross operator to a nine-element pixel subset has been introduced by Sobel.[2] In this technique a two-dimensional nonlinear edge detector is applied to 3 X 3 regions of the image. The edge detection measure for the Sobel operator, $S(x,y)$, is defined as

---

[1] Roberts, LG, Machine Perception of Three-dimensional Solids in Optical and Electro-optical Information Processing, JT Tippett et al,editors, MIT Press, Cambridge, MA 1965.

[2] Dudd, RO and Hart, PE, Pattern Classification and Scene Analysis, Wiley, New York, 1973.

$$S(x,y) = [(\text{Vert. Dif.})^2 + (\text{Horz. Dif.})^2]^{1/2} \tag{2-3a}$$

where

$$\begin{aligned}\text{Vert. Dif.} = {} & [I(x+1, y+1) + 2I(x+1, y) + I(x+1, y-1)] - \\ & [I(x-1, y+1) + 2I(x-1, y) + I(x-1, y-1)]\end{aligned} \tag{2-3b}$$

and

$$\begin{aligned}\text{Horz. Dif.} = {} & [I(x-1, y+1) + 2I(x, y+1) + I(x+1, y+1)] - \\ & [I(x-1, y-1) + 2I(x, y-1) + I(x+1, y-1)]\end{aligned} \tag{2-3c}$$

The Sobel edge detection operator provides an edge detection measurement value for the center pixel location for each 3 $\times$ 3 region of the image analyzed.

Both the Roberts and Sobel edge detection operators have been applied to satellite images. Examples obtained with the Sobel operator for a DMSP satellite image are shown in figures 2-3 and 2-4. Figure 2-3 (b) gives the edge map corresponding to the major geographical features and cloud structures in the DMSP image. The intensities in the edge map are the S(x,y) values for each location (exclusive of the borders) in the original image. Note that there is a large dynamic range for the displayed S(x,y) values in the edge map. Areas with weak or no edge content in the original image have low S(x,y) values, and regions with strong edge structures have correspondingly high S(x,y) values. A variation on the basic method for displaying the Sobel edge detection measures is shown in figure 2-4. In this example, the computed S(x,y) values were compared against a threshold. S(x,y) values exceeding the threshold are displayed at a fixed intensity level in the edge map of figure 2-4 (b), while S(x,y) values less than the threshold are eliminated. Thresholding of Sobel edge detection measures in an interactive mode of operation provides a useful technique for isolating strong or weak edge structures within an image.

MEDIAN FILTERS

The concept of median filtering was first introduced by Tukey.[3] Median filters are a class of nonlinear processing techniques primarily intended for spatial noise suppression and artifact removal in digital imagery.

Both one- and two-dimensional implementations of median filters have been developed. The one-dimensional form of the median filter is comprised of an odd length sequence of horizontally or vertically adjacent pixel values. The action of the median filter is to replace the center pixel value of the sequence with the median of the pixel values within the sequence. By definition, the median of an odd length sequence of length N is that element for which (N-1)/2 of the sequence elements are smaller or equal in value and the remaining (N-1)/2 elements are larger or equal in value.

Examples of applying a one-dimensional median filter of length five to a variety of signal types are illustrated in figure 2-5 (a) through 2-5 (e). In these examples it can be seen that the median filter does not alter the simple step and ramp functions

[3] Tukey, JW, Exploratory Data Analysis, Addison-Wesley, Reading MA, 1971.

(a) Original Image

(b) Edge Map

Figure 2-3. Application of nonlinear Sobel edge detection operator to DMSP satellite image. The edge map indicates the location and relative strength of all edges detected in the image.

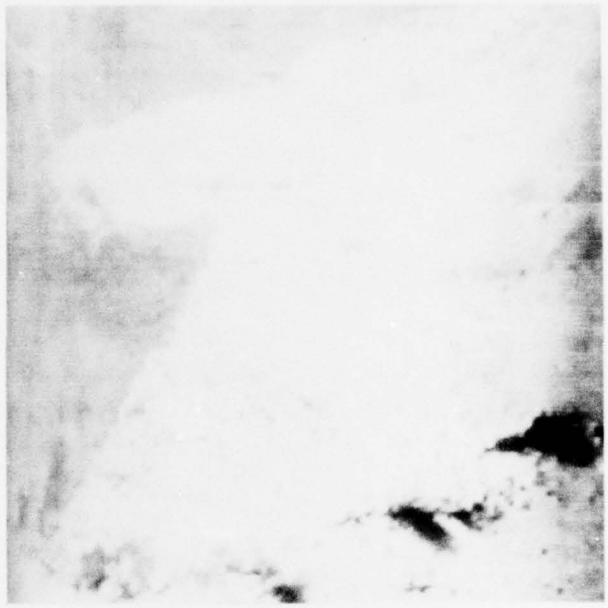

(a) Original Image

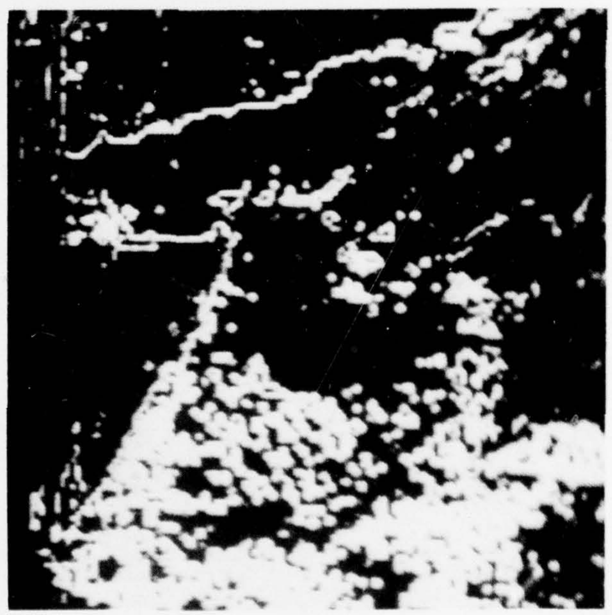

(b) Image Edge Map with Thresholding

Figure 2-4. Application of nonlinear Sobel edge detection operator to DMSP satellite image. Threshold edge map shows all detected edges for which the Sobel edge detection measure exceeded a threshold value.

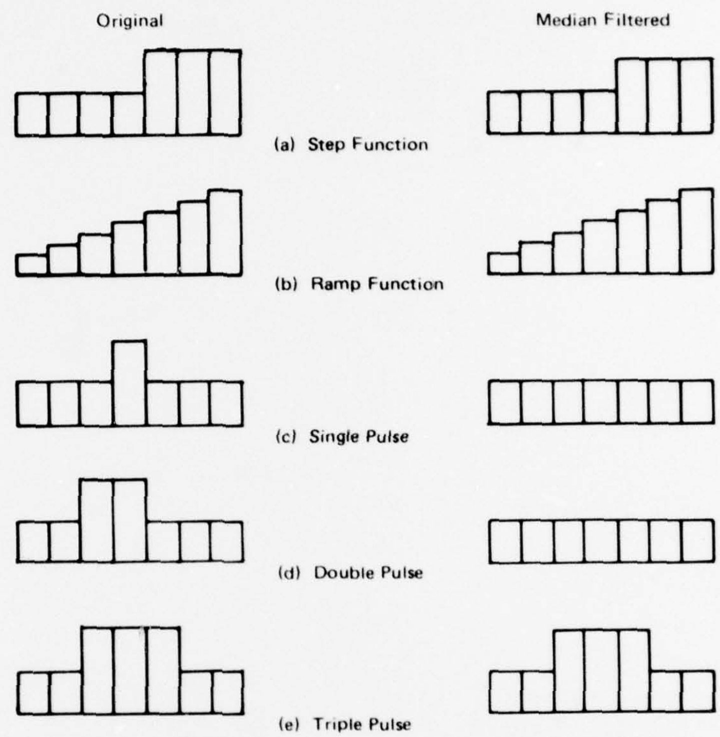

Figure 2-5. Application of one-dimensional median filter of length five to various signal types.

but does successfully eliminate pulse functions whose extent is less than one-half of the length of the median filter sequence.

Extension of median filtering to two dimensions requires the specification of intersecting horizontal and vertical odd length sequences. For two-dimensional median filtering, the center value is replaced by the median value of the combined set of elements in the horizontal and vertical sequences.

A refinement to two-dimensional median filtering is to allow different length sequences in the horizontal and vertical directions. An example of this approach is shown in figure 2-6 where a two-dimensional median filter of extent five elements horizontally and nine elements vertically was used to remove the dot pattern introduced by the optical system of the sensor. Thus, in addition to spatial noise suppression applications, two-dimensional median filters can be satisfactorily used for specialized situations such as removing imaging artifacts.

DISCRETE CONVOLUTION FILTERS

The class of discrete convolution filters permits the application of low pass and high pass spatial domain filters to imagery data. Convolution is of fundamental importance in many signal processing applications and provides a link between operations performed in the spatial domain and in the Fourier transform spatial frequency domain.

(a) Original Image

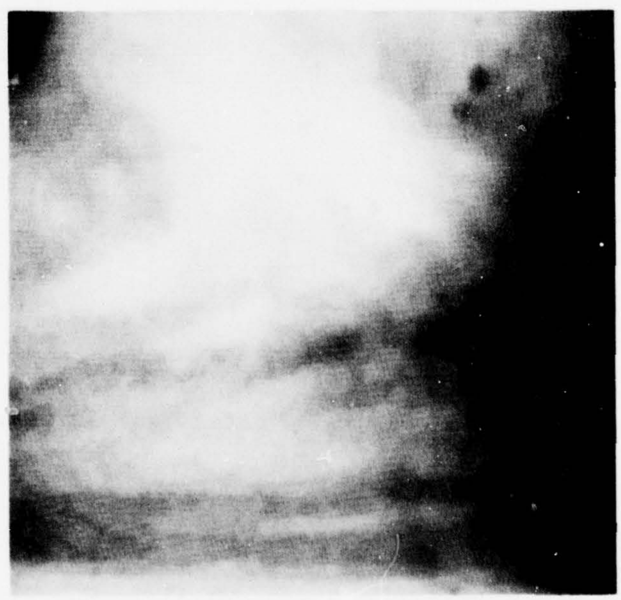

(b) Median Filtered Image

Figure 2-6. Application of two-dimensional median filter of length five horizontally and nine vertically to remove imaging system artifacts from Pioneer flyby image of cloud structures on Venus.

The convolution of two spatial domain functions, f(x,y) and g(x,y) is given by

$$f(x,y) * g(x,y) = \int_{-\infty}^{\infty} f(\alpha, \beta) g(x-\alpha, y-\beta)\, d\alpha\, d\beta \tag{2-4}$$

where α and β are dummy variables of integration. The discrete representation of the convolution relationship is

$$f(x,y) * g(x,y) = \sum_{m=0}^{M-1} \sum_{n=0}^{N-1} f(m,n)\, g(x-m, y-n) \tag{2-5}$$

for x = 0, 1,..., M-1 and y = 0, 1,..., N-1, where f(x,y) and g(x,y) are discrete arrays of size A × B and C × D, respectively, and M and N are chosen according to M = A + C − 1 and N = B + D − 1 to avoid wraparound errors in the convolution periods of f(x,y) and g(x,y).

By letting f(x,y) be the pixel intensity values within image arrays of size A × B, direct image convolution computations can be made for arbitrary g(x,y) filter kernel arrays. Representative g(x,y) kernels for high pass convolutional filtering include

$$g_{HP}(x,y) = \begin{bmatrix} 0 & -1 & 0 \\ -1 & 5 & -1 \\ 0 & -1 & 0 \end{bmatrix} \tag{2-6a}$$

$$g_{HP}(x,y) = \begin{bmatrix} -1 & -1 & -1 \\ -1 & 9 & -1 \\ -1 & -1 & -1 \end{bmatrix} \tag{2-6b}$$

and

$$g_{HP}(x,y) = \begin{bmatrix} 1 & -2 & 1 \\ -2 & 5 & -2 \\ 1 & -2 & 1 \end{bmatrix} \tag{2-6c}$$

These filter kernels have the property that the sum of their elements is unity and, therefore, they do not introduce an intensity bias within each filtered 3 × 3 image array.

Figure 2-7 illustrates the application of the high pass filter kernel of eq. 2-6a to the DMSP satellite image. In the filtered image all local intensity transitions or edges have been enhanced by relatively suppressing the low-frequency components in the image.

The concept of discrete convolution filtering can also be used for image edge enhancement by application of low pass filters. Example low pass filter kernels include

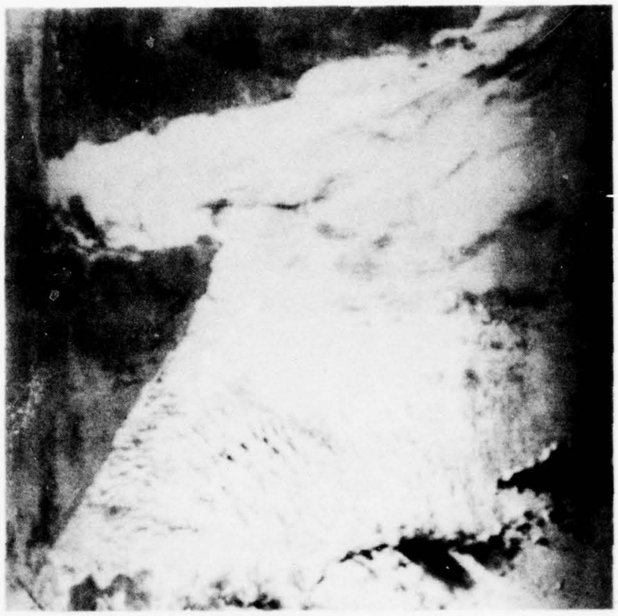

(a) Original Image

(b) High Pass Filtered Image

Figure 2-7. Application of high pass discrete convolution filter to DMSP satellite image. An enhancement of edges within the image results from high pass filtering.

$$g_{LP}(x,y) = 1/9 \begin{bmatrix} 1 & 1 & 1 \\ 1 & 1 & 1 \\ 1 & 1 & 1 \end{bmatrix}, \tag{2-7a}$$

$$g_{LP}(x,y) = 1/10 \begin{bmatrix} 1 & 1 & 1 \\ 1 & 2 & 1 \\ 1 & 1 & 1 \end{bmatrix} \tag{2-7b}$$

and

$$g_{LP}(x,y) = 1/16 \begin{bmatrix} 1 & 2 & 1 \\ 2 & 4 & 2 \\ 1 & 2 & 1 \end{bmatrix} \tag{2-7c}$$

In these kernels, the scaling factor provides local normalization so that the low pass filtering operation does not introduce an intensity bias in the filtered image.

In certain circumstances, the filter kernel can be extended beyond the 3 X 3 array size shown in eq 2-7. For example, figure 2-8 illustrates the application of a low pass convolution filter kernel of the form of eq 2-7a for an array size of 7 X 7 and a scaling factor of 1/49.

By comparison of the original and low pass filtered versions of the DMSP image used in this example, it can be seen that the effect of low pass filtering is to smooth the DMSP image by eliminating the high spatial frequency image components while preserving local average intensity levels.

UNSHARP MASKING

The technique of unsharp masking for digital images evolved from methods developed for enhancement of edges in photographic imagery. In digital unsharp masking, a low pass filtered version of the image is generated using discrete convolutional filtering or Fourier transform techniques. The low pass image is then subtracted from the original image on a pixel-by-pixel basis. The unsharp masking relationship can be expressed as

$$I_{UM}(x,y) = \lambda I(x,y) - (1 - \lambda)\, I_{LP}(x,y) \tag{2-8}$$

where $I(x,y)$ and $I_{LP}(x,y)$ represent the pixel intensities of the original and low pass filtered images, respectively, and $0 < \lambda < 1$ is a weighting factor.

The basic premise of unsharp masking is that the original image contains both high and low spatial frequency components. Thus, subtracting a weighted low pass filtered version of the image from the original will leave a residue image with emphasized high spatial frequency components and a resultant enhancement of edges.

The main variable in the unsharp masking technique is the value used for the weighting factor, λ. From eq 2-8, it can be seen that for near unity values of λ, only slight edge enhancement will occur since the emphasis is placed on the contribution of the original image. Conversely, small λ values will greatly exaggerate edge structures in the resulting image. Figure 2-9 shows various edge enhancement effects on the DMSP

(a) Original Image

(b) Low Pass Filtered Image

Figure 2-8. Application of low pass discrete convolution filter to DMSP image. The result of low pass filtering is a smoothed representation of the original image.

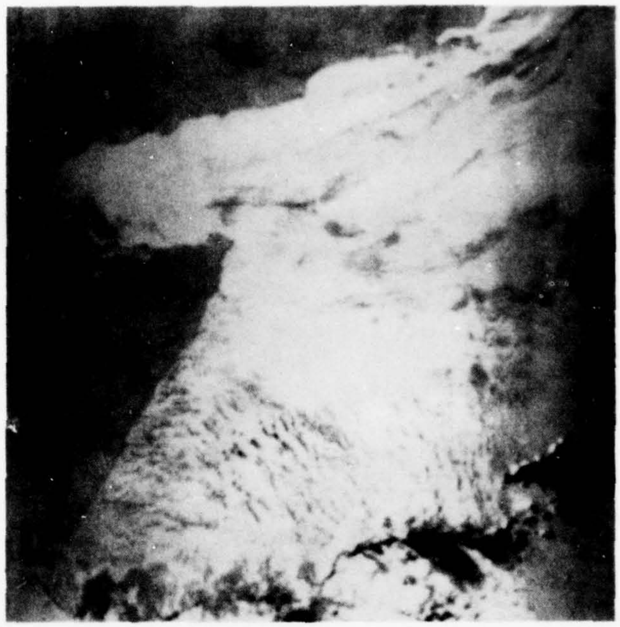

(a) Original Image, $\lambda = 1.0$

(b) $\lambda = 0.65$

Figure 2-9. Unsharp masking technique for edge enhancement applied to the DMSP satellite image. The degree of edge enhancement is increased for smaller values of the λ weighting factor.

(c) λ = 0.55

(d) λ = 0.51

Figure 2-9. Continued.

image for different values of the λ weighting factor. Figure 2-9 (a) illustrates a λ value of 1.0 which corresponds to the original image with no enhancement. In figures 2-9 (b) through 2-9 (d) the weighting factor λ is decreased to show increasing effects of high spatial frequencies. In particular, figure 2-9 (d) gives a nearly equal weighting ($\lambda = 0.51$) to the original and low pass filtered images, which leaves essentially only the edge structure of the image.

TWO-DIMENSIONAL FOURIER TRANSFORMS

The two-dimensional Fourier transform decomposes imagery data in terms of horizontal and vertical spatial frequency components. The display and interpretation of the spatial frequency representation of an image is a valuable tool for detecting and measuring periodicities in spatial image patterns. The mathematical formulations for two-dimensional transforms of images are presented in appendix B.

As opposed to discrete convolutional filters which operate on successive local subarrays of an image, transform techniques generally deal with entire images or large image subarrays. Thus, detection and enhancement operations for low frequency spatial patterns that extend over large portions of an image are generally performed using transform domain techniques rather than the localized spatial domain convolution kernels.

Two examples of Fourier transform decompositions of NOAA satellite images of cloud patterns are shown in figures 2-10 and 2-11. In these examples, the original satellite image is shown in the upper left quadrant. The outlined area within this quadrant indicates the transformed region of the image. The upper right quadrant shows the magnitude of the two-dimensional Fourier transform. Transform phase information is not displayed in this format. An expanded view about the origin in the transform domain is shown in the lower right quadrant. Measurements of the horizontal and vertical spatial frequencies and orientation of a selected spatial pattern in the original image are shown in the lower quadrant.*

In figure 2-10, a NOAA satellite image is shown with a predominant spatial feature in the outlined section consisting of large diagonally oriented cloud formations. The Fourier transform decomposition shows high magnitude intensity concentrations at the low spatial frequencies with little high spatial frequency content. Measured pattern parameters for the magnitude concentrations corresponding to one of the major image patterns are displayed in the lower left quadrant. By way of comparison, the cloud patterns in the NOAA image of figure 2-11 contain numerous periodicities in their spatial patterns. This fact is also reflected in the transform domain decomposition by the presence of a large number of transform magnitude concentrations at different spatial frequency locations. Measured pattern parameters for the energy concentration corresponding to one of the major image patterns are also displayed in this example.

---

* The Fourier transform domain display formats of figures 2-10 and 2-11 are an adaptation of formats developed for the display and analysis of various types of acoustic signal space imagery as described in NOSC TR 337, Two-dimensional Processing for Acoustic Signal Space Imagery, by JA Roese, December 1978.

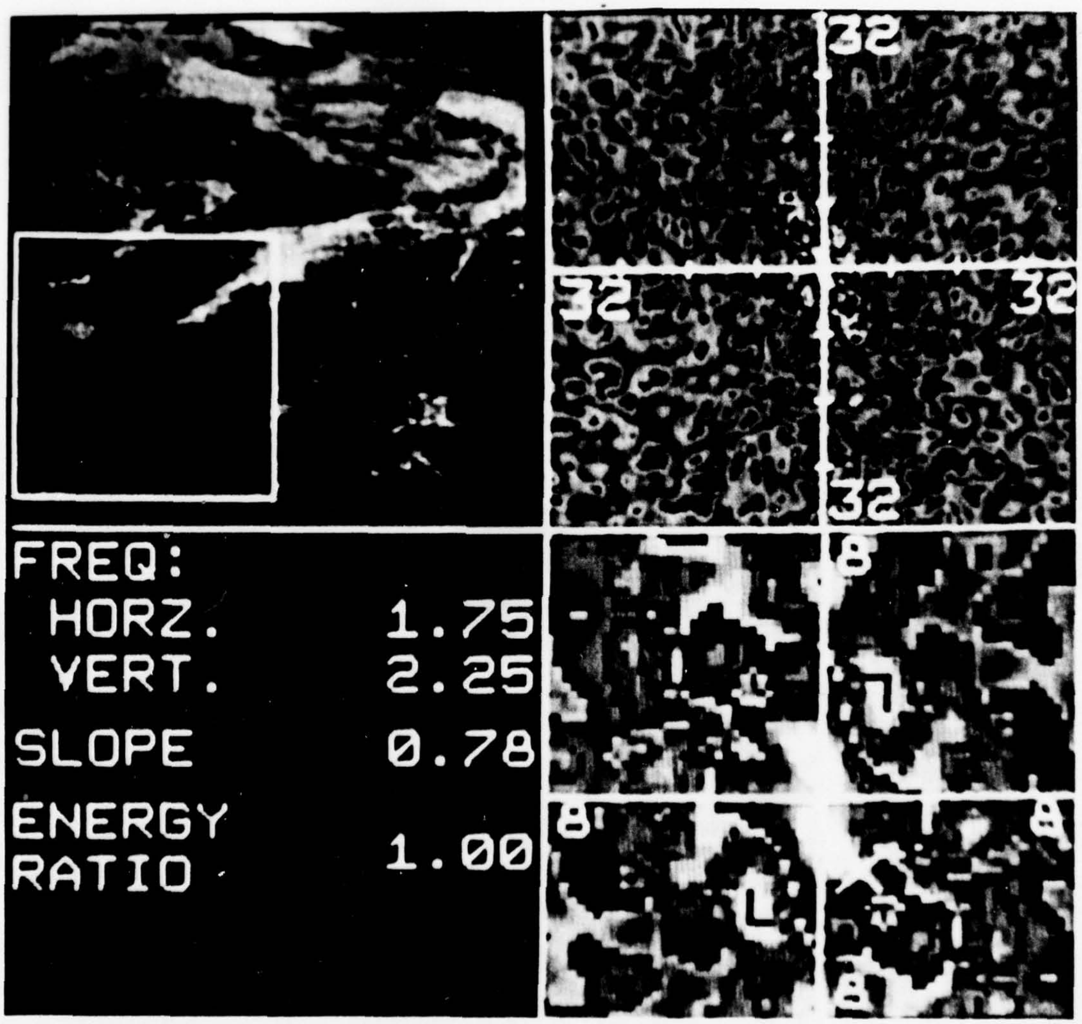

Figure 2-10. Two-dimensional Fourier transform decomposition of NOAA satellite image cloud patterns. Low spatial repetition rate cloud patterns result in transform domain magnitude concentrations at the low spatial frequencies.

In the section on discrete convolution filters, the convolution of two functions, $f(x,y)$ and $g(x,y)$, in the spatial domain was presented. Using discrete convolutional filtering, low pass and high pass filters were discussed. An important property of Fourier transform techniques is that the results of convolution in the spatial domain can also be achieved by direct multiplication in the transform spatial frequency domain. If the Fourier transforms of $f(x,y)$ and $g(x,y)$ are $F(u,v)$ and $G(u,v)$ respectively, then the spatial domain convolution $f(x,y)*g(x,y)$ has the Fourier transform $F(u,v)G(u,v)$. Likewise, convolution of $F(u,v)$ and $G(u,v)$ in the frequency domain reduces to multiplication in the spatial domain. Thus, the discrete spatial domain convolution low pass and high pass filtering operations described previously are equivalent to multiplicative filtering operations performed in the Fourier transform spatial frequency domain. A mathematical development of high pass, low pass, band pass, and band reject spatial frequency filtering is given in appendix C.

SECTION 3. SATELLITE IMAGE DISPLAY TECHNIQUES

Two classes of techniques for the display of satellite images are presented in this section. The first technique deals with the simultaneous display of information gained from concurrent sensor scans in different spectral bands. In particular, an adaptation of field-sequential techniques for stereoscopic CRT displays is presented for simultaneous viewing of combined visible and IR spectrum satellite imagery.

The second display technique also uses the field-sequential stereoscopic display concept. However, in this case, proper geometric positioning and synchronous operation of sensors on two separate geostationary satellites is used to generate true left and right perspective visible spectrum images. From these stereo pairs, actual cloud height measurements can be made.

These display techniques provide the meteorologist or other image analyst with new methods for visually correlating observed cloud structures with both temperature and cloud height information derived directly from satellite imagery.

MULTISPECTRAL STEREOSCOPIC DISPLAYS

Images from satellites such as DMSP, LANDSAT, and NOAA typically result from coincident sensor scans taken in different spectral bands. Different portions of the electromagnetic spectrum have unique properties which permit specialized types of imagery analysis. For example, visible spectrum sensors primarily detect reflected energy, while IR sensors can detect many types of thermal activities, including cloud temperature, heat pollution, and even geothermal activity.

A technique for the simultaneous display of geographically coincident images from two spectral bands is used which is based on the concept of field-sequential stereoscopic CRT displays. In this display technique, the observer perceives depth-of-field due to local horizontal displacements between two images when displayed in an alternating fashion.

In conventional stereoscopic imagery, horizontal displacements between the left and right images are due to the object geometry as viewed from two slightly different sensor or camera perspectives. However, with the use of simple computer algorithms, horizontal displacement can also be synthetically produced, which results in stereoscopically complementary pairs of images. Further, these synthetically produced displacements can be a function of a totally independent variable such as temperature.

As a case in point, geographically coincident visible and IR spectrum satellite images have been displayed using the synthetic stereo technique. In this technique, the visible spectrum image is displayed with horizontal displacements introduced at each pixel location in proportion to the IR temperature reading at that location. The visual effect of the synthetic stereo technique is that the viewer simultaneously observes cloud reflectivity and cloud temperature information over the entire sensor's field of view where the temperature variable is encoded as the perceived displacement of the cloud structures from the surface of the CRT screen. For the display of combined visible/IR spectrum images, the temperature range of the clouds is presented in such a manner that the coldest clouds appear to be displaced farthest above the CRT screen. The temperature range for land and water masses within the sensor field of view is modified to produce a realistic zero displacement from the CRT screen.

The computer algorithm for generating synthetic stereo images treats the visible spectrum image intensity values on a pixel-by-pixel basis. Due to the nature of the field sequential technique used for displaying the stereoscopic images, horizontal displacements for IR temperature values are all introduced in one direction along the odd numbered image rows (displayed during one field scan) and in the other direction for the even numbered image rows (displayed for the interlace field scan). The amount of horizontal displacement for each intensity value is proportional to the IR temperature reading at that pixel location and ranges from zero to a maximum of 16 pixels in either direction.

In the horizontal displacement process, consideration must be given to situations in which two intensities are assigned to the same pixel location and to the problem of gaps created in the image data. In the first case, an intensity precedence scheme is used in which only the highest value assigned to a given pixel location is retained. For filling in gaps created in the data, replication of the nonzero pixel intensity value adjacent to the gap and opposite to the direction of horizontal displacement is used.

Examples of the use of the field-sequential synthetic stereo technique to generate combined visible/IR spectrum images are shown in figures 3-1 and 3-2. It should be noted that, although synthetic stereo horizontal displacements in the cloud structures are present, no depth-of-field is experienced from the photographs in these figures. However, when these images are displayed on a CRT in a normal field sequential mode and viewed with electro-optic shutter viewers synchronized with the field scan rate, strong depth-of-field sensations of cloud height are achieved.

Left and right perspective and field-sequential composite synthetic stereo images for a combined visible/IR NOAA satellite image are shown, respectively, as figures 3-1 (a) (b) and (c). These images show a large storm system with extreme cloud temperature variations centered over the continental United States. An interactive three-coordinate cursor has been incorporated into the synthetic stereo display format to permit direct cloud temperature measurements to be taken. Geographical coordinates corresponding to the location of the cursor are also provided. The cloud temperatures are obtained by visually positioning the three-coordinate cursor to have the same apparent displacement from the CRT screen as a given cloud structure. The temperature measurements obtained and geographic location are displayed at the upper left of the image. Representative latitude, longitude, and cloud temperature measurements for these images are illustrated in the examples of figures 3-1 and 3-2.

(a) Left Perspective Image

(b) Right Perspective Image

Figure 3-1. Composite visible/IR spectrum NOAA satellite image displays using synthetic stereo technique. Horizontal displacements correspond to encoded IR temperature information and give a depth-of-field effect when the image is viewed with electro-optic shutter stereoscopic viewers.

(c) Field-sequential Composite Image

Figure 3-1. Continued.

Additional examples of field-sequential composite visible/IR spectrum images are presented in figure 3-2 (a) and (b). These images present two scenes from a six-image sequence of NOAA visible and IR images recorded at thirty-minute intervals in time. Time sequencing of satellite images is a commonly used meteorological technique for tracking cloud system movements and inferring wind velocity vectors. As illustrated in this figure, the technique of synthetic stereoscopic displays can be used in conjunction with conventional time sequence analysis methods to provide the meteorologist with the additional parameter of IR spectrum information.

VISIBLE SPECTRUM STEREOSCOPIC DISPLAYS

The use of exclusively visible spectrum satellite imagery of cloud structures is also of great importance in meteorological studies. For example, measurements taken from cloud positions in image sequences recorded at thirty-minute intervals have been particularly useful for inferring wind velocity vectors. The addition of cloud height information with the wind velocity vector estimates can lead to improved models for studying wind patterns.

Direct measurements of cloud height have been made from images recorded in a near-simultaneous fashion by two geostationary satellites. Figure 3-3 shows a field-sequential composite of perspective images taken by visible spectrum sensors on the SMS1 and SMS2 satellites over the southeastern United States. As opposed to the synthetic stereo technique discussed in the previous section, the depth-of-field effect achieved with the images from the pair of geostationary satellites is due to the near-simultaneous generation of two geometrically correct visible spectrum perspective images.

Figure 3-3 also illustrates the use of the interactive three-coordinate cursor. In this case, however, the cursor is used to measure actual cloud height instead of cloud temperature. The height measurement is made by positioning the cursor at the same displacement from the CRT screen as the cloud structure being measured. The cloud height is read out along with the geographical coordinates of the cursor location.

SECTION 4. CONCLUSIONS

The intent of this program has been to demonstrate the use of selected image processing and display techniques for multispectral satellite imagery. The image processing techniques investigated provide the remote sensing image analyst with a variety of easily implemented methods for image intensity rescaling, detection of edges, and removal of certain types of image artifacts and spatial noise. Comparisons drawn between filtering operations performed in the spatial domain of the original image and the transform spatial frequency domain indicate that spatial domain convolution techniques should be used for image patterns of large extent.

The adaptation of field-sequential stereoscopic techniques for displaying composite visible/IR spectrum satellite images as well as perspective visible spectrum images has been successfully demonstrated. The use of the three-coordinate cursor as an interactive aid for determining cloud height and temperature information has also been shown to have potential for meteorological image analysis applications.

(a) Field-sequential Composite of First Image

(b) Field-sequential Composite of Second Image

Figure 3-2. Two images from a time sequence of combined visible/IR spectrum NOAA satellite images displayed using synthetic stereo technique. This example illustrates the combination of multispectral stereoscopic and time-sequence techniques for the display of satellite imagery.

Field-sequential Composite Image

Figure 3-3. Example of visible spectrum SMS1 and SMS2 satellite images for cloud height measurements. When displayed using field-sequential stereoscopic techniques, the cloud structures are displaced above the CRT screen.

APPENDIX A – DISPLAY AND IMAGE PROCESSING LABORATORY

BACKGROUND

The NOSC Display and Image Processing Laboratory shown in figure A-1 is a user oriented research facility for the analysis and display of digital and video imagery. The Laboratory is directly linked to the UNIVAC 1108 computer and to the Signal Processing Evaluation Laboratory (SPEL). The SPEL PDP 11/70 host computer, SPS-81 signal processor, and other associated data handling and storage facilities are available resources for Display and Image Processing Laboratory activities. To date, the facilities of the Display and Image Processing Laboratory have been used in a variety of applications for the display of natural and computer-processed images and real-time video. Displays of computer-processed imagery include numerous format options for presentations of surveillance sonar data, situation displays for system performance prediction, and deformation modeling of sonar transducers. Natural image displays include digitized multispectral satellite imagery, encoded aerial reconnaissance sequences, and X-ray fluoroscopy. In addition, laboratory resources include a three-dimensional real-time color video system. This system has been used with a NOSC unmanned submersible work vehicle to evaluate three-dimensional video in an operational undersea environment. Other Laboratory activities include research programs on two-dimensional processing techniques for digital image analysis and enhancement and computer-generated stereoscopic imagery.

DISPLAY HARDWARE

Display and output devices in the Display and Image Processing Laboratory include:

- RAMTEK 9400 high resolution graphics and imagery display system
- COMTAL 8300 digital image display system
- Digital-to-Video image conversion system
- MAGNAVOX color television cameras (2 units)
- HONEYWELL stereoscopic viewers (3 units)
- SONY 2850 editing video tape recorder
- SONY color monitors (2 units)
- TEKTRONIX 4014 graphics display terminal
- NIKON and POLAROID cameras
- GAMMA SCIENTIFIC spectro-radiometric instrumentation

The principal Laboratory display devices are the RAMTEK 9400 and COMTAL 8300 digital image and graphics display systems. These systems provide a wide range of user options for display and interactive manipulation of high-resolution monochrome and color imagery and computer graphics. Pertinent features of the RAMTEK and COMTAL systems include:

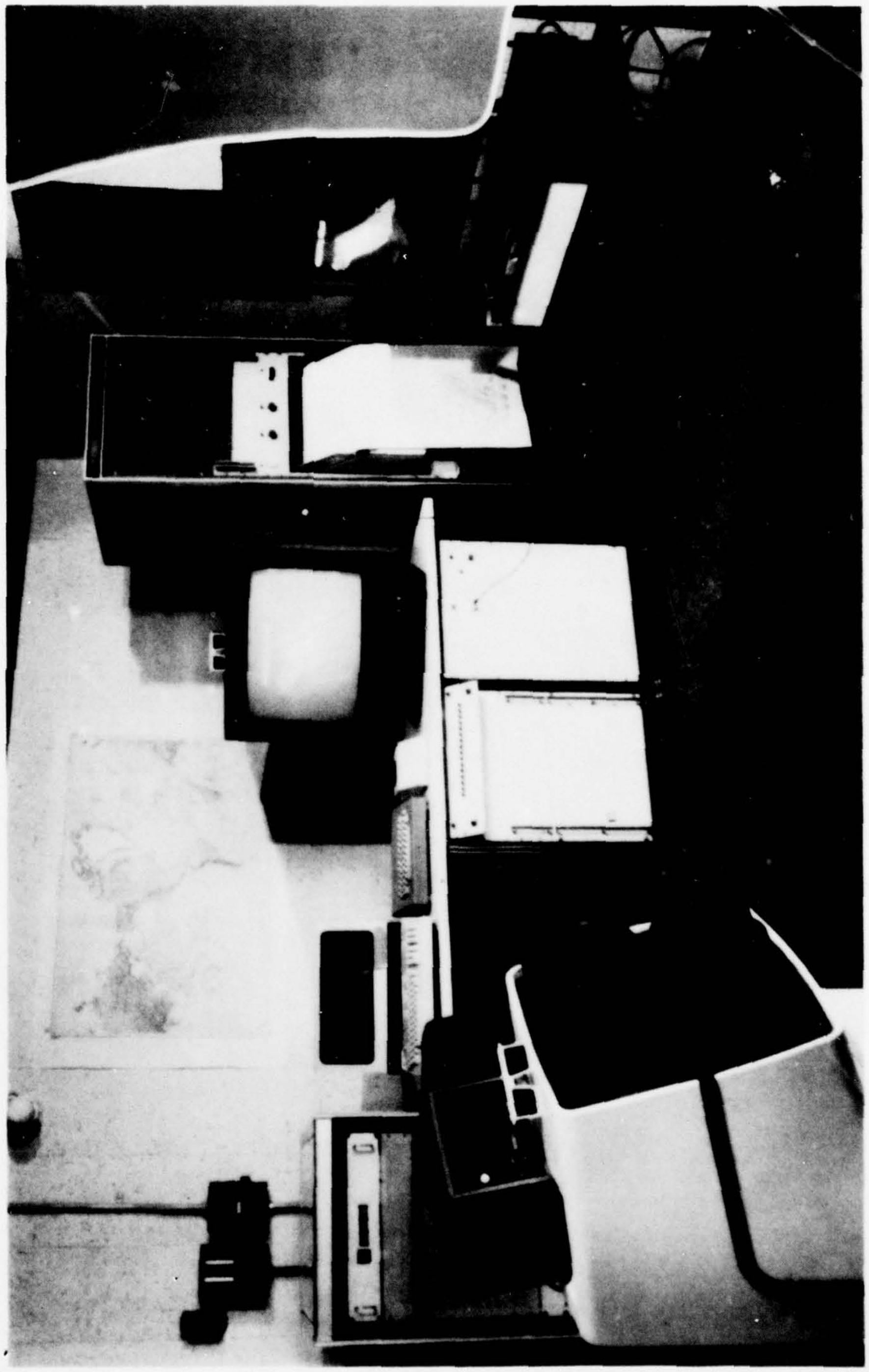

Figure A-1. Display and Image Processing Laboratory.

RAMTEK 9400

- Dual 256 level 1024 X 1024 picture element monochrome display monitors
- RGB (16 levels/color) 1024 X 1024 picture element color display monitor (750 X 750 effective resolution)
- 1024 X 1024 16-bit refresh memory assignable to the three display monitors
- 128K byte display processor
- 3 eight-bit video generators
- 4 cursors assignable to the display monitors
- Graphics capability including vectors, conic sections, and text with pan, zoom, scroll and blink
- 32K X 32K virtual image transformations including translation, scaling and clipping
- Trackball and alphanumeric keyboard inputs

COMTAL 8300

- 512 X 512 picture element resolution with a 1:1 aspect ratio
- Selectable data display modes, including gray scale, pseudo-color, and true color
- Three independent images stored at one time
- Eight bits of intensity coding stored for each pixel (six bits displayed)
- Graphics overlay for superimposing outlines, grids, or alphanumerics on display images
- Trackball positioning of a target pointer using a trackball input control device.

In conjunction with the COMTAL display, a digital-to-video image conversion system has been developed for producing NTSC compatible color video tape cassettes of images displayed on the COMTAL. Tapes produced on this system can be played on any standard video playback/monitor unit. With this digital-to-video conversion capability, results of current display simulations or experiments can be made available for immediate presentations outside of the laboratory.

DISPLAY AND IMAGE PROCESSING SOFTWARE

Extensive user-oriented software has been developed in support of Display and Image Processing Laboratory activities. An operating system supported by a library of FORTRAN callable user routines has been written for the COMTAL 8300 system. Using this system, highly interactive operations involving data retrieval and editing, alphanumeric and graphic overlay generation, trackball target control, and image manipulation using function memory modification can be performed on demand terminals located in the Laboratory area. In addition, many user application routines exist, including algorithms for transform and spatial domain image processing, continuous tone graphics, automatic scoring and analysis of experiments, and image formatting for computer-processed and natural images, stereoscopic imagery and high-refresh-rate loading of image sequences.

In the area of image processing, applications software has been developed to perform one- and two-dimensional discrete Fourier, cosine and Hadamard unitary transforms. This software has been designed for interactive operator specification of transform domain filtering operations using two-dimensional low-pass, high-pass, band-reject and band-pass filters. Frequency domain filtering can be used for image noise removal and feature enhancement such as improving edge or contour definition. Algorithms have also been implemented for processing in the original image domain. These methods include techniques for image domain spatial noise removal, edge enhancement, and contrast enhancement.

The SPEL PDP 11/70 and UNIVAC 1108 host computers can be accessed from demand terminals located within the Display and Image Processing Laboratory. These host computer facilities offer bulk data storage (disc, drum, 7- and 9-track tape), high level operating systems (UNIX, EXEC-8), a selection of standard compilers, and complete mathematical and plotter user libraries (e.g., IMSL, DISSPLA).

APPENDIX B: MATHEMATICAL FORMULATIONS FOR TWO-DIMENSIONAL TRANSFORMS

GENERAL FORMS

The general forms for the two-dimensional forward and inverse transformations of an image array are given in Equations (B-1) and (B-2). The two-dimensional transform of an N × N image array is itself an N × N array of transform domain coefficients. The forward two-dimensional transform operation is

$$F(u,v) = \sum_{x=1}^{N} \sum_{y=1}^{N} f(x,y)\, a(x,y,u,v) \qquad \text{(B-1)}$$

where $a(x,y,u,v)$ is the forward transform kernel and x,y and u,v are, respectively, image domain and transform domain coordinates. The inverse transform is given by

$$f(x,y) = \sum_{u=1}^{N} \sum_{v=1}^{N} F(u,v)\, a^{-1}(x,y,u,v) \qquad \text{(B-2)}$$

where $a^{-1}(x,y,u,v)$ is the inverse transform kernel.

The transform kernel $a(x,y,u,v)$ is called separable if it can be expressed in the form

$$a(x,y,u,v) = a_x(x,u)\, a_y(y,v) \qquad \text{(B-3)}$$

Computationally, transform kernel separability means that a two-dimensional transform of an image can be performed by first applying a one-dimensional transform along the rows of $f(x,y)$

$$F(u,y) = \sum_{x=1}^{N} f(x,y)\, a_x(x,u) \qquad \text{(B-4)}$$

followed by another one-dimensional transform along the columns of $F(u,y)$ which yields $F(u,v)$, i.e.,

$$F(u,v) = \sum_{y=1}^{N} F(u,y)\, a_y(y,v) \qquad \text{(B-5)}$$

Thus, transformations of two-dimensional image arrays reduce to the application of sequential one-dimensional transform algorithms along the rows and columns of the image array.

FOURIER TRANSFORMS

An important class of unitary transformation is the Fourier transform. For this transform, the general forms for the forward and inverse transforms become

$$\mathscr{F}(u,v) = \frac{1}{N^2} \sum_{x=1}^{N} \sum_{y=1}^{N} f(x,y) \exp\left[\frac{-2\pi i}{N}(ux + vy)\right] \quad \text{(B-6)}$$

and

$$f(x,y) = \sum_{u=1}^{N} \sum_{v=1}^{N} \mathscr{F}(u,v) \exp\left[\frac{2\pi i}{N}(ux + vy)\right] \quad \text{(B-7)}$$

The two-dimensional discrete Fourier transform can be computed using sequential one-dimensional transform algorithms since its transform kernel is separable and symmetric, i.e.,

$$\exp\left[\frac{2\pi i}{N}(ux + vy)\right] = \exp\left[\frac{2\pi i}{N} ux\right] \exp\left[\frac{2\pi i}{N} vy\right] \quad \text{(B-8)}$$

Unitary transformations result in the projection of an image into a new orthogonal vector space. In the case of the discrete Fourier transform, the vector space basis functions are complex exponentials.

APPENDIX C – SPATIAL FREQUENCY FILTERS

GENERAL FORM

The general form for the reconstruction of an image after transform domain filtering is

$$\hat{f}(x,y) = \sum_{u=1}^{N} \sum_{v=1}^{N} F(u,v)\, a^{-1}(x,y,u,v)\, \beta(u,v) \qquad \text{(C-1)}$$

where $\hat{f}(x,y)$ is the filtered image reconstruction and $\beta(u,v)$ is a two-dimensional set of filter weights. The values assumed by the filter weights determine the spatial features that are eliminated, enhanced, or in some way modified in the reconstructed version of the image.

LOW-PASS FILTER

For the simple case of two-dimensional low-pass spatial frequency filtering, $\beta(u,v)$ has the form

$$\beta_{LP}(u,v) = \begin{cases} 1 & \begin{matrix} u \leq U_{Low} \\ v \leq V_{Low} \end{matrix} \\ 0 & \text{otherwise} \end{cases} \qquad \text{(C-2)}$$

where U_{Low} and V_{Low} define the bounds for the spatial frequency components used in the image reconstruction. In low-pass filtering, the image reconstruction no longer contains horizontal and vertical spatial frequency components exceeding U_{Low} and V_{Low}. The resulting visual effect of low-pass spatial frequency filtering is a general smoothing of the reconstructed image since the higher spatial frequency components have been removed.

HIGH-PASS FILTER

In a similar fashion, high-pass spatial frequency filtering can be obtained with weights of the form

$$\beta_{HP}(u,v) = \begin{cases} 1 & \begin{matrix} U_{High} \leq u \\ V_{High} \leq v \end{matrix} \\ 0 & \text{otherwise} \end{cases} \qquad \text{(C-3)}$$

Visually, the result of high-pass spatial frequency filtering is that the bias and low-frequency components less than U_{High} and V_{High} have been removed, leaving just the outlines of image intensity transitions. In the context of the analysis and enhancement of natural images, high-pass filtering is commonly used for edge detection and line enhancement purposes.

BAND-PASS FILTER

The properties of low-pass and high-pass filters can be combined to form two-dimensional band-pass spatial frequency filters. The band-pass filter weights are

$$\beta_{BP}(u,v) = \begin{cases} 1 & \begin{matrix} U_{Low} \leqslant u \leqslant U_{High} \\ V_{Low} \leqslant v \leqslant V_{High} \end{matrix} \\ 0 & \text{otherwise} \end{cases} \tag{C-4}$$

Band-pass filtering is a powerful processing tool because it permits individual image features to be isolated from the remainder of the image. The isolated features of the image can then be analyzed and measured to determine their respective contributions to the original image. Simultaneous implementation of multiple band-pass filters can be used to analyze interactions between combinations of specific spatial features within the image.

BAND-REJECT FILTER

The complement of band-pass filtering is band-reject filtering. The expression for two-dimensional band-reject filter weights is

$$\beta_{BR}(u,v) = \begin{cases} 0 & \begin{matrix} U_{Low} \leqslant u \leqslant U_{High} \\ V_{Low} \leqslant v \leqslant V_{High} \end{matrix} \\ 1 & \text{otherwise} \end{cases} \tag{C-5}$$

This form of spatial frequency filtering allows selective removal of image features while preserving the basic structure of the residual image. By means of this technique, image features attributable to known phenomena can be effectively eliminated to permit an unobscured view of the signal structures of primary interest.

PATTERN MODIFICATION

A special case of spatial frequency filtering are those filters that permit relative adjustments to be made in individual patterns or spatial features of the image. These filters permit variable enhancement or suppression of specific image features by the use of weights of the form

$$\beta_{PM}(u,v) = \begin{cases} \psi & \begin{matrix} U_{Low} \leqslant u \leqslant U_{High} \\ V_{Low} \leqslant v \leqslant V_{High} \end{matrix} \\ 1 & \text{otherwise} \end{cases} \tag{C-6}$$

where $\psi > 1$ results in increased values for the selected components in the transform domain energy distribution and $\psi > 1$ causes a corresponding compone it value decrease. Such distortions of the transform domain energy distribution produces, respectively, increases or decreases in the perceived strength of the affected features in the image reconstruction. Pattern modification is a potentially powerful image processing tool which can be used to enhance weak features or suppress undesirable ones for subsequent image feature analysis and measurement.

ENERGY RATIO MEASUREMENT

The techniques of spatial frequency filter provide a direct method for evaluating the relative strength of individual spatial features within the source image. The energy ratio measurement has the form

$$\text{Energy Ratio} = \frac{\sum_{u=o}^{N} \sum_{v=0}^{N} |F(u,v)| \beta(u,v)}{\sum_{u=0}^{N} \sum_{v=0}^{N} |F(u,v)|} \tag{C-7}$$

where $\beta(u,v)$ is the set of filter weights discussed previously. The numerator of Equation (C-7) represents the energy of a particular feature after filtering, while the denominator is the total energy of the source image. This fractional energy ratio is one of the feature parameters displayed in the lower left quadrant of the spatial frequency filtering display format.